

Environment-Assisted Quantum Transport in a 10-qubit Network

Christine Maier,^{1,2} Tiff Brydges,^{1,2} Petar Jurcevic,^{1,2} Nils Trautmann,^{3,†} Cornelius Hempel,^{1,2,4}
Ben P. Lanyon,^{1,2} Philipp Hauke,^{5,6} Rainer Blatt,^{1,2} and Christian F. Roos^{1,2,*}

¹*Institute for Quantum Optics and Quantum Information, Austrian Academy of Sciences,
Technikerstr. 21A, 6020 Innsbruck, Austria*

²*Institute for Experimental Physics, University of Innsbruck, Technikerstr. 25, 6020 Innsbruck, Austria*

³*Institute for Applied Physics, TU Darmstadt 64289, Germany*

⁴*ARC Centre of Excellence for Engineered Quantum Systems, School of Physics,
University of Sydney, Sydney, NSW 2006, Australia*

⁵*Kirchhoff-Institute for Physics, Heidelberg University, 69120 Heidelberg, Germany*

⁶*Institute for Theoretical Physics, Heidelberg University, 69120 Heidelberg, Germany*



(Received 27 September 2018; published 8 February 2019)

The way in which energy is transported through an interacting system governs fundamental properties in nature such as thermal and electric conductivity or phase changes. Remarkably, environmental noise can enhance the transport, an effect known as environment-assisted quantum transport (ENAQT). In this Letter, we study ENAQT in a network of coupled spins subject to engineered static disorder and temporally varying dephasing noise. The interacting spin network is realized in a chain of trapped atomic ions, and energy transport is represented by the transfer of electronic excitation between ions. With increasing noise strength, we observe a crossover from coherent dynamics and Anderson localization to ENAQT and finally a suppression of transport due to the quantum Zeno effect. We find that in the regime where ENAQT is most effective, the transport is mainly diffusive, displaying coherences only at very short times. Further, we show that dephasing characterized by non-Markovian noise can maintain coherences longer than white noise dephasing, with a strong influence of the spectral structure on the transport efficiency. Our approach represents a controlled and scalable way to investigate quantum transport in many-body networks under static disorder and dynamic noise.

DOI: [10.1103/PhysRevLett.122.050501](https://doi.org/10.1103/PhysRevLett.122.050501)

Introduction.—The transport of energy through networks governs fundamental phenomena such as light harvesting in photosynthetic organisms [1,2] or properties of nano-fabricated quantum devices [3,4]. Often, such systems are subject to static disorder, which for noninteracting particles suppresses transport through Anderson localization [5]. In realistic networks, coupling to environments such as phonon baths moreover induces dynamical noise that can lift Anderson localization, an effect known as environment-assisted quantum transport (ENAQT). This phenomenon has been postulated to be a key factor enabling the high efficiency of energy conversion in photosynthetic biomolecules [6–9]. At large noise levels, the transport efficiency again decreases due to the quantum Zeno effect [10]. While the general phenomenology governing the transport efficiency is widely accepted, many works have been dedicated to understanding the influence of non-Markovian noise [11–15] as well as coherence [6,13,16–21]. Here, engineered quantum systems provide a prime opportunity, by enabling controlled studies of energy transport under noisy environments. Recent experiments have started investigating the elementary building blocks of ENAQT but were limited to, at most, four network nodes, represented by photonic waveguides, classical electrical oscillators, superconducting qubits, or trapped ions [22–27].

In this Letter, we study ENAQT in a controlled network of 10 coupled spins subject to static disorder and dephasing noise [see inset (a) in Fig. 1]. The network is realized in a system of trapped ions following a recent proposal [28]. Our approach enables us to investigate the role of ENAQT in a controlled quantum network that does not have a simple lattice structure restricted to close-neighbor interactions. First, applying white dephasing noise of increasing strength, we observe a crossover from coherent dynamics and Anderson localization to ENAQT, and finally a suppression of transport due to the quantum Zeno effect. In the regime where ENAQT is most effective, we find that the transport reveals coherences only at very short times and that the spread of the excitation is mostly diffusive. Finally, we show that non-Markovian dephasing can maintain coherences longer than white noise, with a strong influence of the structure of the noise spectrum on the transport efficiency.

Experimental implementation.—Experimental Implementation The nodes of our quantum network are encoded into (pseudo-) spin- $\frac{1}{2}$ particles, represented by two internal electronic states of $^{40}\text{Ca}^+$ ions trapped in a linear Paul trap [32]. We define the state $|S_{\frac{1}{2}}, m = +\frac{1}{2}\rangle$ as spin down $|\downarrow\rangle$ and $|D_{\frac{3}{2}}, m = +\frac{5}{2}\rangle$ as spin up $|\uparrow\rangle$. A spin-spin interaction Hamiltonian is realized by global laser pulses coupling the

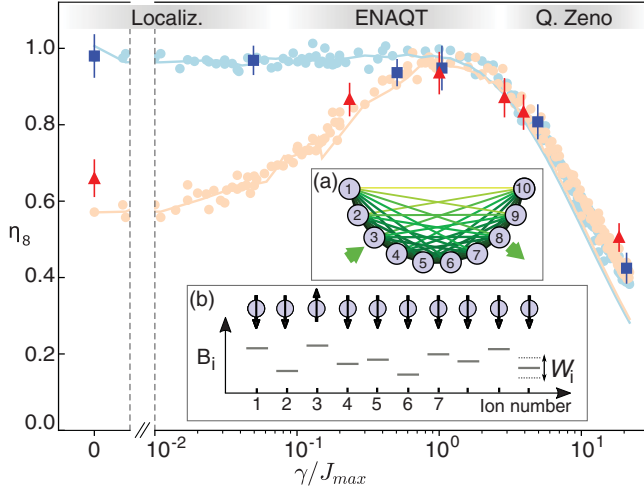


FIG. 1. Main graph: Transport efficiency η_8 to the target (ion 8) under different strengths of static disorder (blue: $B_{\max} = 0.5J_{\max}$; red: $B_{\max} = 2.5J_{\max}$) and Markovian-like dephasing with rate γ . Experimental points (shown as dark squares and triangles) result from averaging over 20–40 random realizations of disorder and noise, with 25 experimental repetitions each. Error bars are derived via bootstrapping, based on 1000 samples (see [29] for details). The regimes of localization, ENAQT, and the quantum Zeno effect are indicated in gray. The data agree well with theoretical simulations of the coin-tossing random process (light bullets) realized in the experiment, while simulations with ideal Markovian white noise (lines) underestimate ENAQT at large γ . The simulation averages over 300 random realizations. Inset (a): Sketch of the transport network. The ions experience a long-range coupling, with darker and thicker connections indicating higher coupling strengths. The green arrows denote the source (3) and the target (8) for the excitation in the ion network. Inset (b): Sketch of the ion chain representing interacting spin- $1/2$ particles as blue circles, with the spin states denoted by black arrows. The ions are subject to random static and dynamic on-site excitation energies, indicated by B_i and $W_i(t)$.

electronic states of all ions [33,34]. In the subspace with a single spin excitation $|\uparrow\rangle$, the Hamiltonian is given by

$$H_1 = \hbar \sum_{i \neq j} J_{ij} (\sigma_i^+ \sigma_j^- + \text{H.c.}). \quad (1)$$

Here, σ_i^+ (σ_i^-) are the spin raising (lowering) operators for site i . This Hamiltonian describes the hopping of spin excitations between sites i and j and conserves the total magnetization; i.e., the number of spins in the excited state $|\uparrow\rangle$ is preserved. The hopping rates follow an approximate power law, $J_{ij} = J_{\max}/|i-j|^\alpha$, with peak strength J_{\max} between $(2\pi)28$ Hz and $(2\pi)33$ Hz and exponent $\alpha = 1.22$ [33]. Inset (a) of Fig. 1 depicts this quantum network.

Static disorder, disturbing the quantum network, is represented as on-site excitation energies $\hbar B_i$ [see Fig. 1(b) and Eq. (3)]. The values B_i are randomly sampled from a uniform distribution $[-B_{\max}, B_{\max}]$, with $B_{\max} \in \{0.5, 2.5\}J_{\max}$. In the experiment, these disorder energies are realized by laser beams focused to single ions and introducing precisely

controlled ac-Stark shifts on the encoded spin states [35]. For this, we apply multiple radio frequencies to an acousto-optical deflector, generating a set of laser beams to simultaneously address multiple ions.

Moreover, we can temporally modulate the ac-Stark shifts, employing an arbitrary-wave-form generator with a switching time much faster than all other timescales. Using this technique, we are able to engineer time-dependent on-site energies $\hbar W_i(t)$, which induce dephasing between the $|\downarrow\rangle$ and $|\uparrow\rangle$ states. In this way, we simulate a stationary noise process with vanishing mean, $\langle\langle W_i(t) \rangle\rangle = 0$, and broadly tunable spectral power [36,37]

$$S(\omega) = \lim_{T \rightarrow \infty} \frac{1}{T} \int_0^T \int_0^T \langle\langle W_i(t) W_i(t') \rangle\rangle e^{i\omega(t-t')} dt' dt, \quad (2)$$

where $\langle\langle \cdot \rangle\rangle$ denotes averaging over noise trajectories. Cross talk between neighboring spins and subharmonics of the driving frequencies are negligible, so noise at different sites is uncorrelated. Including static disorder and dynamical dephasing noise, the Hamiltonian H_1 becomes

$$H = \hbar \sum_{i \neq j} J_{ij} (\sigma_i^+ \sigma_j^- + \text{H.c.}) + \hbar \sum_i (B_i + W_i(t)) \sigma_i^z, \quad (3)$$

where σ^z is the Pauli- z matrix.

To investigate ENAQT, we introduce an excitation at time $t = 0$ at the source site $i_{\text{source}} = 3$ [see inset (a) of Fig. 1] by preparing spin i_{source} in the σ_i^z eigenstate $|\uparrow\rangle$ while keeping all other spins in the eigenstate $|\downarrow\rangle$. We observe the transport of the excitation through the network to the target site $i_{\text{target}} = 8$ under the Hamiltonian H in Eq. (3), for both Markovian and non-Markovian dephasing. The source and target sites are chosen such that the transport dynamics is not immediately influenced by boundary effects. We define the transport efficiency to a particular site i by $\eta_i \equiv \int_0^{t_{\max}} dt p_i(t)$. Here, $p_i(t) = (\langle\sigma_i^z(t)\rangle + 1)/2$ is the instantaneous probability to find the excitation at site i and $t_{\max} = 60$ ms $\approx 11.7/J_{\max}$ is the system's evolution time. The time is chosen such that the evolution is long enough to observe ENAQT and short enough to minimize decoherence from amplitude damping due to spontaneous decay [28]. Any residual amplitude damping effect is eliminated by postselecting measurements with a single excitation in the system. Typically, more than 77% of the measurements lie within this subspace.

Markovian dephasing.—Markovian dephasing We first study ENAQT in the regime where $W_i(t)$ can be described as white (or Markovian) noise, i.e., $S(\omega) = \text{const}$. In the experiment, every $\Delta T = 100$ μs (200 μs) we randomly sample W_i between $\{-(W_{\max}/2), (W_{\max}/2)\}$ with equal probabilities (equivalent to tossing a coin). As the “coin-tossing rate” $\lambda = 1/\Delta T$ is much faster than the maximal hopping J_{\max} , over the relevant frequency range this process is well approximated as white noise $S(\omega) = (W_{\max}^2/\lambda)$. This constant spectral power defines the noise strength and gives a rate of dephasing $\gamma = (W_{\max}^2/\lambda)$. We apply dephasing noise to our system under

(i) weak static disorder $B_{\max} = 0.5J_{\max}$ and (ii) strong static disorder $B_{\max} = 2.5J_{\max}$.

Figure 1 shows the measured transport efficiency η_8 as a function of γ/J_{\max} : Weak static disorder $B_{\max} < J_{\max}$ (blue markers) does not affect transport considerably. However, with additional noise at a level beyond $\gamma = J_{\max}$, the transport efficiency gradually decreases. This regime, where noise is the dominant effect and it inhibits quantum transport, is known as the quantum Zeno regime. Under strong static disorder $B_{\max} > J_{\max}$ (red markers), the phenomenology becomes even richer: At weak dephasing, $\gamma < J_{\max}$, excitation transport is suppressed corresponding to Anderson localization. Around $\gamma \approx J_{\max}$, the noise cancels destructive interference causing the localization, and it thereby enhances the transport efficiency, which is the hallmark of ENAQT. For strong noise, $\gamma > J_{\max}$, the quantum Zeno effect again suppresses transport.

The experimental results agree well with theoretical simulations of the coin-tossing random process (light bullets in Fig. 1). At very strong dephasing, the shift W_{\max} becomes comparable to the coin flipping rate λ , and the Markovian approximation is no longer fulfilled. In this case, deviations from ideal Markovian white noise (lines) become noticeable, as discussed in [28]. Such non-Markovian effects will be further discussed later, after analyzing the coherence properties of the quantum transport.

Coherent dynamics in excitation transport.—The role of coherences in ENAQT has been discussed in the context of exciton transport in photosynthetic complexes [9,38–41]. To investigate how coherences affect excitation transport in our system, we observe the time-resolved dynamics of the excitation probability of spin 8, $p_8(t)$, for strong static disorder and several levels of dephasing noise (see Fig. 2). Without dephasing noise, $\gamma = 0$, oscillations are distinctive by a few standard deviations, indicating quantum coherent transport. In the intermediate regime $\gamma \sim J_{\max}$, however, the spurious oscillations are on the order of statistical fluctuations. A theoretical model with ideal Markovian noise reflects the transition to a classical rate equation, valid for $t \gg 1/\gamma$ (see Supplemental Material [42]). For strong dephasing noise, the excitation dynamics is well described by this classical rate equation (see Fig. 2). Here, the coherences between sites have been adiabatically eliminated, resulting in the equation

$$\dot{p}_i = \sum_{\ell \neq i} \Gamma_{\ell i} (p_{\ell} - p_i), \quad (4)$$

with $p_i(t)$ the excitation probability of spin i . The classical hopping rate $\Gamma_{\ell i} = \{(\gamma J_{i\ell}^2)/[4(B_i - B_{\ell})^2 + \gamma^2]\}$ is derived from the experimental spin-spin coupling matrix $J_{i\ell}$, B_i are the applied static on-site energies, and γ is the dephasing noise rate. This set of coupled differential equations describes a purely diffusive transport of the spin excitation. For weak dephasing, we observe deviations from rate equation (4) at short times, which indicates a temporal

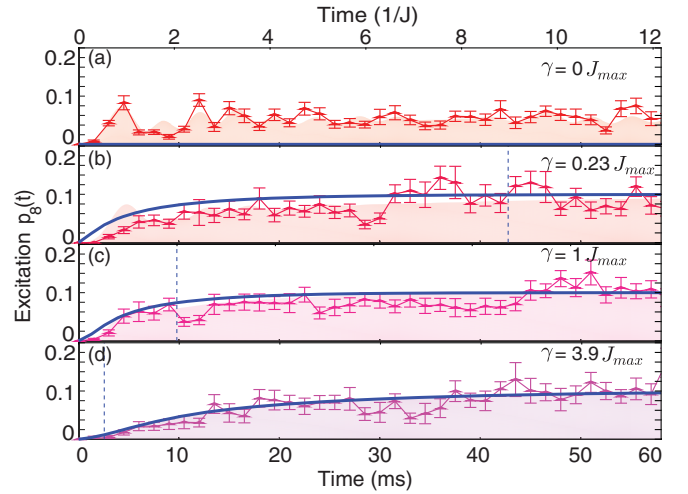


FIG. 2. Excitation probability at ion 8 as a function of time, for strong static disorder $B_{\max} = 2.5J_{\max}$ and increasing dephasing rate, from (a) to (d), $\gamma/J_{\max} = 0|0.23|1|3.9$. Each data set (red to magenta triangles) results from averaging over 20–40 random realizations, with 25 repetitions each. Error bars are derived with bootstrapping [29], based on 1000 samples. With increasing γ , coherent oscillations damp out, and the data converge towards a model following diffusive, classical rate equations (blue solid line). This theoretical approximation is valid for times $t \gg 1/\gamma$. (The crossover $t_c = 1/\gamma$ is illustrated by a blue dashed line.) Shaded areas show the time evolution of a theoretical model with ideal Markovian noise, averaged over 100 random realizations.

crossover from ballistic to diffusive transport, similar to what has recently been resolved in classical Brownian motion [43]. With increasing dephasing strength, the observed coherences are damped, and the system converges to a diffusive rate equation. This highlights the fact that Anderson localization is a wave phenomenon caused by destructive interference, which is lifted by dephasing.

Crossover from ballistic to subdiffusive transport.—We can quantify the transport behavior by examining the spatial dispersal of the excitation, i.e., by measuring the spatial width σ_{WP} of the excitation wave packet. This analysis is analogous to experiments with ultracold atoms in a momentum space lattice [44] and to experiments in a photonic system on a discrete quantum walk [45]. We calculate the width via the spread from source spin i_3 : $\sigma_{\text{WP}}(t) \approx \sqrt{2(\sum_{i>i_3} p_i(t)(i - i_3)^2)}$ (this formula is chosen to reduce boundary effects; see Supplemental Material [42] for details). Depending on the relationship to time, $\sigma_{\text{WP}}(t) \propto t^C$, one distinguishes between “normal diffusion” as it occurs in classical random walks ($C = 0.5$), “subdiffusion” ($0 < C < 0.5$), and “superdiffusion” ($C > 0.5$). The case $C = 1$ is referred to as ballistic transport. As we now show, we observe ballistic, diffusive, and subdiffusive behavior in our experiment.

The excitation dynamics $p_i(t)$ for three exemplary parameter values is displayed in the left column of Fig. 3. At small

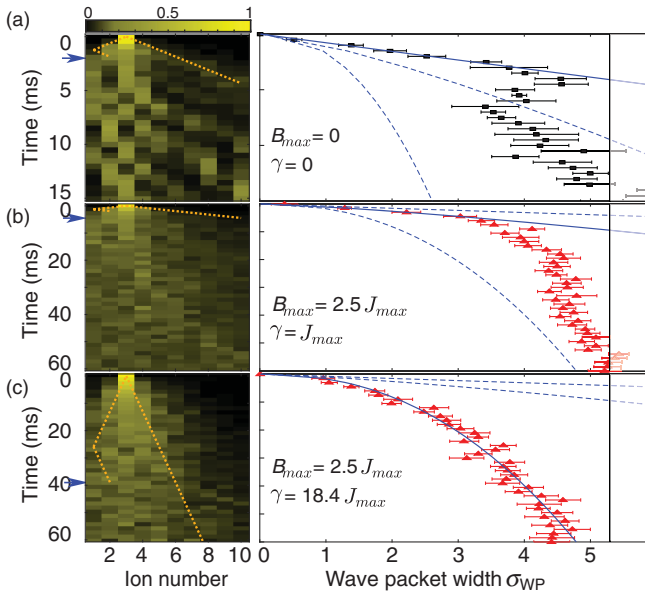


FIG. 3. Left panels: Single-ion resolved excitation dynamics $p_i(t)$ for (a) the unperturbed system (no static disorder and no noise), (b) static disorder $B_{\max} = 2.5J_{\max}$ with dephasing $\gamma = J_{\max}$, and (c) static disorder $B_{\max} = 2.5J_{\max}$ with $\gamma = 18.4J_{\max}$. The orange dotted line shows the maximum speed at which an excitation spreads (see Supplemental Material [42]) in order to estimate until when the reflection from the left boundary can be neglected (blue arrows). Right panels: Spatial width of the excitation wave packet $\sigma_{\text{WP}}(t)$, calculated from the data in the left panels. Blue solid lines are fits of the form $\sigma_{\text{WP}} = At^C$ (fits from the respective other panels are included as dashed lines for comparison). The vertical black line at $\sigma_{\max} = 5.3$ is the expected maximum of the wave-packet width, for a single excitation distributed equally over all ions. (a) $A = 6.5 \pm 0.5, C = 1.05 \pm 0.06$, (b) $A = 3.2 \pm 0.3, C = 0.74 \pm 0.17$, (c) $A = 1.7 \pm 0.1, C = 0.44 \pm 0.02$. All error bars are derived via bootstrapping [29], based on 100 samples.

γ , an interference pattern is clearly visible. This hallmark for coherence is rapidly washed out as γ increases. We fit a power law of the form $\sigma_{\text{WP}}(t) = At^C$ to the width of the wave packet (see Fig. 3, right column), only including data up to the time where the excitation has been reflected from the left boundary back to ion 2 (Fig. 3, left column). In this way, we exclude data dominated by boundary effects. Without any disorder and noise, the width increases linearly in time with $C = 1.05 \pm 0.06$, corresponding to ballistic spreading. In the regime around $\gamma = J_{\max}$ [Fig. 2(b)], where ENAQT is most efficient, we find that within very short times $t \sim 1/J_{\max}$, the transport evolves from ballistic to mainly diffusive dynamics (as theoretically predicted in Ref. [46]), yielding $C = 0.74 \pm 0.17$.

For strong dephasing, $\gamma = 18.4J_{\max}$, we observe subdiffusive transport with a power exponent $C = 0.44 \pm 0.02$. Based on theoretical simulations, we conclude that subdiffusive dynamics is caused by the long-range interactions in our system.

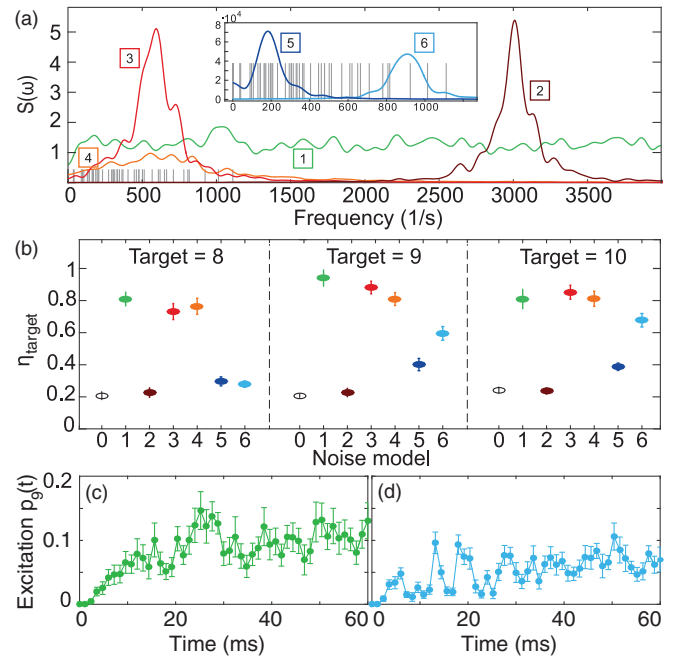


FIG. 4. Comparison of different noise models. (a) Spectral density functions $S(\omega)$ of (1) white noise and (2)–(6) non-Markovian noise models of Lorentzian shape. The curves are averaged over about 30 random realizations, each generated by a Gaussian random process based on 600 sampling points. The inset shows a zoom into the low-frequency domain. Vertical grey lines denote the difference frequencies between all eigenenergies of the disordered system. (b) Comparison of η_{target} to target ions 8–10 subject to strong static disorder and the noise models shown in (a), as indicated by corresponding colors and numbering. Noise model zero indicates bare static disorder without noise. While broadband noise in the correct frequency range generically enhances transport efficiencies, for narrow-band noise the enhancement depends on the source and target ions. Each data point results from averaging over 25–30 random realizations, with 15 repetitions each. Error bars are derived with bootstrapping [29], based on 1000 samples. (c,d) Excitation probability of target ion 9 as a function of time under strong static disorder and different noise models. Panel (c) shows the result for the Markovian noise model (1). Oscillations, indicating coherent dynamics, are strongly damped. Panel (d) shows the effects of a narrow-band Lorentzian noise model covering only a few eigenstates (model 6). Here, coherences are more strongly maintained and are clearly discriminable from measurement errors up to about 30 ms.

Non-Markovian dephasing.—In Fig. 1, the experimentally observed transport efficiencies for $\gamma > J_{\max}$ are higher than the simulated values for ideal Markovian noise. This discrepancy could indicate that non-Markovian effects can increase the transport efficiency. To investigate non-Markovian dephasing further, we study ENAQT under noise with a spectral density function $S(\omega)$ of Lorentzian shape, which we generate using the frequency-domain algorithm described in Ref. [47]. We choose a single random configuration of static disorder ($B_{\max} = 2.5J_{\max}$) in order to have full knowledge of the disordered system and its eigenvalues.

From Fig. 4, we see that the spectral structure of the noise model has a strong influence on the transport efficiency: Non-Markovian structured noise that covers all difference frequencies of the spin system's eigenenergies (models 3 and 4) can enhance excitation transport as much as white noise (model 1), and the efficiency is similar for different target ions [Fig. 4(b)]. Narrow-band noise models, instead, only couple a few eigenstates, so the spectral position determines for which target ions excitation transport is enhanced (cf. models 5 and 6 in Fig. 4). Integrating the applied local energy shifts over the entire interaction time, we find that with narrow-band non-Markovian noise, we can achieve similar transport efficiencies as with Markovian noise but already at half the energy cost [cf. noise models 1 and 6 in Fig. 4(a)]. Further, panels (c) and (d) in Fig. 4 show that coherences can be maintained better for narrow-band noise models than for Markovian-like noise.

Conclusion.—We have experimentally analyzed a quantum network under static disorder and dynamic noise, realized in a string of 10 trapped ions. We observed effects of Anderson localization in the absence of noise, an increased transport efficiency by ENAQT at intermediate noise levels, and, finally, suppression of quantum transport under strong noise due to the quantum Zeno effect. Further, we have found that coherences play a role only in the localized regime (at very low noise strengths) or at very short times. In all other regimes of Markovian noise, the dynamics is well captured through a diffusive rate equation describing a classical random walk. Finally, we found that the structure of non-Markovian dephasing strongly influences quantum transport, with the possibility to reach as large efficiencies as with white noise while maintaining long-lived coherences.

In the future, it will be interesting to study the possibility of stochastically accelerated hypertransport, generated, e.g., by time-evolving disorder [48]. Further, our approach allows one to investigate quantum transport with multiple interacting excitations or to study localization using out-of-time-ordered correlators (OTOCs) [49,50].

This Letter was supported by Deutsche Forschungsgemeinschaft (DFG) as part of the CRC 1119 CROSSING, by the DFG Collaborative Research Centre SFB 1225 (ISOQUANT), and by the European Research Council (ERC) under the European Union's Horizon 2020 Research and Innovation Programme (Grant Agreement No. 694561, Entangle-Gen).

*Corresponding author.
christian.roos@uibk.ac.at

†Present address: Carl Zeiss AG, 73447, Oberkochen, Germany.

- [1] R. E. Blankenship, *Molecular Mechanisms of Photosynthesis* (Wiley-Blackwell, Oxford, 2002).
[2] R. J. Sension, *Nature (London)* **446**, 740 (2007).

- [3] S. Sho and S. Odanaka, *J. Comput. Phys.* **235**, 486 (2013).
[4] J. Lee, A. O. Govorov, and N. A. Kotov, *Nano Lett.* **5**, 2063 (2005).
[5] P. W. Anderson, *Phys. Rev.* **109**, 1492 (1958).
[6] F. Caruso, A. W. Chin, A. Datta, S. F. Huelga, and M. B. Plenio, *J. Chem. Phys.* **131**, 105106 (2009).
[7] S. Huelga and M. Plenio, *Contemp. Phys.* **54**, 181 (2013).
[8] N. Lambert, Y.-N. Chen, Y.-C. Cheng, C.-M. Li, G.-Y. Chen, and F. Nori, *Nat. Phys.* **9**, 10 (2013).
[9] F. Fassioli, R. Dinshaw, P. C. Arpin, and G. D. Scholes, *J. R. Soc. Interface* **11**, 20130901 (2014).
[10] B. Misra and E. C. G. Sudarshan, *J. Math. Phys. (N.Y.)* **18**, 756 (1977).
[11] M. Thorwart, J. Eckel, J. Reina, P. Nalbach, and S. Weiss, *Chem. Phys. Lett.* **478**, 234 (2009).
[12] X. Chen and R. J. Silbey, *J. Phys. Chem. B* **115**, 5499 (2011).
[13] A. W. Chin, J. Prior, R. Rosenbach, F. Caycedo-Soler, S. F. Huelga, and M. B. Plenio, *Nat. Phys.* **9**, 113 (2013).
[14] M. Mohseni, A. Shabani, S. Lloyd, and H. Rabitz, *J. Chem. Phys.* **140**, 035102 (2014).
[15] S. Jesenko and M. Žnidarič, *J. Chem. Phys.* **138**, 174103 (2013).
[16] G. S. Engel, T. R. Calhoun, E. L. Read, T.-K. Ahn, T. Mančal, Y.-C. Cheng, R. E. Blankenship, and G. R. Fleming, *Nature (London)* **446**, 782 (2007).
[17] H. Lee, Y.-C. Cheng, and G. R. Fleming, *Science* **316**, 1462 (2007).
[18] M. del Rey, A. W. Chin, S. F. Huelga, and M. B. Plenio, *J. Phys. Chem. Lett.* **4**, 903 (2013).
[19] G. Panitchayangkoon, D. Hayes, K. A. Fransted, J. R. Caram, E. Harel, J. Wen, R. E. Blankenship, and G. S. Engel, *Proc. Natl. Acad. Sci. U.S.A.* **107**, 12766 (2010).
[20] M. Mohseni, P. Rebentrost, S. Lloyd, and A. Aspuru-Guzik, *J. Chem. Phys.* **129**, 174106 (2008).
[21] M. B. Plenio and S. F. Huelga, *New J. Phys.* **10**, 113019 (2008).
[22] S. Viciani, M. Lima, M. Bellini, and F. Caruso, *Phys. Rev. Lett.* **115**, 083601 (2015).
[23] D. N. Biggerstaff, R. Heilmann, A. A. Zecevik, M. Gräfe, M. A. Broome, A. Fedrizzi, S. Nolte, A. Szameit, A. G. White, and I. Kassal, *Nat. Commun.* **7**, 11282 (2016).
[24] R. de J. León-Montiel, M. A. Quiroz-Juárez, R. Quintero-Torres, J. L. Domínguez-Juárez, H. M. Moya-Cessa, J. P. Torres, and J. L. Aragón, *Sci. Rep.* **5**, 17339 (2015).
[25] S. Mostame, P. Rebentrost, A. Eisfeld, A. J. Kerman, D. I. Tsomokos, and A. Aspuru-Guzik, *New J. Phys.* **14**, 105013 (2012).
[26] A. Potočník, A. Bargerbos, F. A. Y. N. Schröder, S. A. Khan, M. C. Collodo, S. Gasparinetti, Y. Salathé, C. Creatore, C. Eichler, H. E. Türeci *et al.*, *Nat. Commun.* **9**, 904 (2018).
[27] D. J. Gorman, B. Hemmerling, E. Megidish, S. A. Moeller, P. Schindler, M. Sarovar, and H. Haefner, *Phys. Rev. X* **8**, 011038 (2018).
[28] N. Trautmann and P. Hauke, *Phys. Rev. A* **97**, 023606 (2018).
[29] Bootstrapping is a technique to assign measures of accuracy (e.g., variance) to sample data, and it relies on random sampling with replacement [30,31]. In our experiment, a single data set is composed of L realizations with random disorder and noise. Step (1) of the bootstrapping is to sample

- $L - 2$ realizations from our data set and compute the mean $\bar{\eta}$. Then, step (1) is repeated B times to come up with estimates $\bar{\eta}_1, \bar{\eta}_2, \dots, \bar{\eta}_B$. Finally, the standard deviation of all B estimates corresponds to the standard error of the data set.
- [30] R. W. Johnson, *Teach. Stat.* **23**, 49 (2001).
- [31] B. Efron, *Ann. Stat.* **7**, 1 (1979).
- [32] P. Schindler, D. Nigg, T. Monz, J. T. Barreiro, E. Martinez, S. X. Wang, S. Quint, M. F. Brandl, V. Nebendahl, C. F. Roos *et al.*, *New J. Phys.* **15**, 123012 (2013).
- [33] P. Jurcevic, B. P. Lanyon, P. Hauke, C. Hempel, P. Zoller, R. Blatt, and C. F. Roos, *Nature (London)* **511**, 202 (2014).
- [34] P. Jurcevic, P. Hauke, C. Maier, C. Hempel, B. P. Lanyon, R. Blatt, and C. F. Roos, *Phys. Rev. Lett.* **115**, 100501 (2015).
- [35] J. Smith, A. Lee, P. Richerme, B. Neyenhuis, P. W. Hess, P. Hauke, M. Heyl, D. A. Huse, and C. R. Monroe, *Nat. Phys.* **12**, 907 (2016).
- [36] F. Rieke, W. Bialek, R. De Ruyter van Steveninck, and D. Warland, *Spikes: Exploring the Neural Code* (MIT press, Cambridge, Massachusetts, 1999).
- [37] S. Millers and D. Childers, *Probability and Random Processes* (Academic Press, New York, 2012).
- [38] G. S. Engel, *Procedia Chem.* **3**, 222 (2011).
- [39] I. Kassal, J. Yuen-Zhou, and S. Rahimi-Keshari, *J. Phys. Chem. Lett.* **4**, 362 (2013).
- [40] E. Romero, R. Augulis, V. I. Novoderezhkin, M. Ferretti, J. Thieme, D. Zigmantas, and R. van Grondelle, *Nat. Phys.* **10**, 676 (2014).
- [41] A. Chenu and G. D. Scholes, *Annu. Rev. Phys. Chem.* **66**, 69 (2015).
- [42] See Supplemental Material at <http://link.aps.org/supplemental/10.1103/PhysRevLett.122.050501> for the derivation of the classical rate equation and the calculation of the wave packet width with reduced boundary effects.
- [43] R. Huang, I. Chavez, K. M. Taute, B. Lukić, S. Jeney, M. G. Raizen, and E.-L. Florin, *Nat. Phys.* **7**, 576 (2011).
- [44] F. A. An, E. J. Meier, and B. Gadway, *Nat. Commun.* **8**, 325 (2017).
- [45] A. Schreiber, K. N. Cassemiro, V. Potoček, A. Gábris, I. Jex, and C. Silberhorn, *Phys. Rev. Lett.* **106**, 180403 (2011).
- [46] S. Gopalakrishnan, K. R. Islam, and M. Knap, *Phys. Rev. Lett.* **119**, 046601 (2017).
- [47] D. B. Percival, *Comput. Sci. Stat.* **24**, 534 (1992).
- [48] L. Levi, Y. Krivolapov, S. Fishman, and M. Segev, *Nat. Phys.* **8**, 912 (2012).
- [49] Y. Huang, Y.-L. Zhang, and X. Chen, *Ann. Phys. (Berlin)* **529**, 1600318 (2016).
- [50] C.-J. Lin and O. I. Motrunich, *Phys. Rev. B* **97**, 144304 (2018).